

# Optimization of thermo-mechanical reliability of solder joints in crystalline silicon solar cell assembly

M. T. Zarmai\*, N. N. Ekere, C. F. Oduoza and E. H. Amalu

School of Engineering, Faculty of Science and Engineering,  
University of Wolverhampton, WV1 1LY, UK, \* [m.t.zarmai@wlv.ac.uk](mailto:m.t.zarmai@wlv.ac.uk)

## ABSTRACT

A robust solder joint in crystalline silicon solar cell assembly is necessary to ensure its thermo-mechanical reliability. The solder joint formed using optimal parameter setting accumulates minimal creep strain energy density which leads to longer fatigue life. In this study, thermo-mechanical reliability of solder joint in crystalline silicon solar cell assembly is evaluated using finite element modelling (FEM) and Taguchi method. Geometric models of the crystalline silicon solar cell assembly are built and subjected to accelerated thermal cycling utilizing IEC 61215 standard for photovoltaic panels. In order to obtain the model with minimum accumulated creep strain energy density, the  $L_9 (3^3)$  orthogonal array was applied to Taguchi design of experiments (DOE) to investigate the effects of IMC thickness ( $IMC_T$ ), solder joint width ( $SJ_W$ ) and solder joint thickness ( $SJ_T$ ) on the thermo-mechanical reliability of solder joints. The solder material used in this study is Sn3.8Ag0.7Cu and its non-linear creep deformation is simulated using Garofalo-Arrhenius creep model. The results obtained indicate that solder joint thickness has the most significant effect on the thermo-mechanical reliability of solder joints. Analysis of results selected towards thermo-mechanical reliability improvement shows the design with optimal parameter setting to be: solder joint thickness -  $20\mu\text{m}$ , solder joint width -  $1000\mu\text{m}$ , and IMC thickness -  $2.5\mu\text{m}$ . Furthermore, the optimized model has the least damage in the solder joint and shows a reduction of 47.96% in accumulated creep strain energy density per cycle compared to the worst case original model. Moreover, the optimized model has 16264 cycles to failure compared with the expected 13688 cycles to failure of a PV module designed to last for 25 years.

**Keywords:** Solar cell assembly, Solder joints, Optimization, Thermo-mechanical reliability, Finite element method, Taguchi method

## 1. Introduction

The dominance of wafer-based crystalline silicon photovoltaic (PV) modules over thin-film modules remains strong despite concerted efforts towards production of the latter. The global production of wafer-based crystalline silicon PV modules in 2013 was 90.956% of global module production [1]. Wafer-based crystalline silicon PV modules have the advantage of decades of proven technology, higher efficiency than most of their thin-film competitors, decreasing cost of production as well as increasing demand. Though this trend is expected to continue for a long time, certain aspects of the manufacturing technology of wafer-based crystalline silicon PV modules still need to be improved. The manufacturing process of conventional wafer-based crystalline silicon PV modules involves printing silver (Ag) busbar electrode onto the front surface of silicon solar cell wafer. This process is followed by high temperature soldering of highly conductive solder-coated copper ribbon strip on the printed

46 Ag busbar while an extended part of the ribbon strip is soldered to the back of a neighbouring  
47 cell to form a series connection. The solder joint enables current transfer from the front of  
48 one cell to the back of a neighbouring cell. Additionally, the solder joint in the assembly act  
49 as mechanical support to hold the ribbon strip to the silicon wafer via Ag busbar.  
50 Furthermore, the solder joint function as thermal conduit to dissipate heat away from the  
51 silicon wafer. At the present time, lead-free solder alloys such as tin-silver-copper (SAC)  
52 alloys are used for the interconnection of solar cells instead of the hazardous lead-based  
53 solder alloys which were formerly used.

54  
55 Moreover, crystalline silicon PV modules are expected to last up to 25 years in field  
56 operations. Guyenot et al [2] estimated that for 1.5 thermal cycles per day with a temperature  
57 change of about 50 °C, expected life of solder joints for 25 years is 13688 cycles to failure.  
58 However, the high temperature soldering of these solar cells induces thermo-mechanical  
59 stress in the solder joints thereby diminishing the expected lifespan. In addition, the soldering  
60 results in the diffusion of copper (Cu) and tin (Sn) elements to form intermetallic compound  
61 (IMC) layers at the solder and copper ribbon interface. Likewise, Ag and Sn elements diffuse  
62 to form IMC layers at the solder and Ag busbar interface. The IMC layer formed at the  
63 interface joint between solder and copper ribbon, consists mainly of  $\text{Cu}_3\text{Sn}$  and  $\text{Cu}_6\text{Sn}_5$  IMCs  
64 while at the solder and Ag busbar solder interface joint, the IMC layer consist of  $\text{Ag}_3\text{Sn}$   
65 intermetallic compounds [3]. In the course of field operations, PV modules undergo thermo-  
66 mechanical fatigue loading due to thermal cycling and differences in the coefficient of  
67 thermal expansion (CTE) of the interconnect materials. The result of the thermal effect is  
68 further growth of the IMCs in the solder joint which is detrimental to the solder joint fatigue  
69 life [4]. In an experimental study, Schmitt et al [3] reported that IMCs decrease the  
70 performance and reliability of solder joints in PV modules. Moreover, as the solder joint  
71 undergoes isothermal aging, the IMC thickness increases. Also, the fatigue loading creates  
72 creep deformation in the solder joint. The deformation is stored internally throughout the  
73 volume of solder joint as creep strain energy. Creep strain energy per unit volume of material  
74 is referred to as creep strain energy density. As IMC thickness increases, solder joint volume  
75 decreases and more creep strain energy density accumulates in the solder joint. Eventually  
76 resulting in fatigue failure of the solder joints such that the larger the accumulated creep  
77 strain energy density, the shorter the fatigue life. Therefore, minimal accumulated creep  
78 strain energy density in the solder joint is desirable as its decrease means the enhancement of  
79 thermo-mechanical reliability which leads to longer fatigue life. One of the ways of  
80 minimizing accumulated creep strain energy density is through minimizing IMC thickness in  
81 the solder joint. Hence, IMC thickness is a factor which affects the thermo-mechanical  
82 reliability of solder joint and should be taken into consideration when optimizing the  
83 parameter setting of the joint.

84  
85 Other factors which also need to be considered for optimization are solder joint design  
86 parameters particularly solder joint thickness and solder joint width. It is desirable that solder  
87 joint width is minimized to reduce shadowing losses because the wider the solder joint, the  
88 wider the shadow on the solar cell and the lesser the amount of current generated by the solar  
89 cell. Conversely, the solder joint thickness should have adequate capacity to transfer  
90 generated current to the desired point. It is desirable that optimal solder joint thickness and  
91 width are used such that minimal accumulation of creep strain energy density occurs in the  
92 solder joint in order to enable longer fatigue life.

93  
94 Usually, accelerated thermal cycling (ATC) tests are used to experimentally determine the  
95 thermo-mechanical reliability of a package [5]. However, the process consumes time and is  
96 costly. A better option is numerical analysis of thermo-mechanical reliability of devices as  
97 performed by several researchers such as Ladani [6] and Yang et al [7]. Such numerical

98 evaluation enables faster, low-cost and efficient determination of thermo-mechanical  
99 reliability of solder joints before the device or product is manufactured. Furthermore, the use  
100 of the concept of design of experiment (DOE) facilitates robust design of solder joints  
101 thereby enhancing thermo-mechanical reliability of solder interconnects. There are numerous  
102 DOE tools in use, yet, Taguchi method is popularly used because it is aimed at improving  
103 quality as well as allowing the effects of several factors to be determined simultaneously and  
104 efficiently [8]. Application of Taguchi method for DOE in this research enables the selection  
105 of the best matching combination of geometric parameters for improving the thermo-  
106 mechanical reliability of solder joints under thermal cycling.

107  
108 In this study, finite element modelling (FEM) and Taguchi method for DOE are employed to  
109 evaluate the thermo-mechanical reliability of solder joints with various sets of parameters and  
110 subjected to thermal cycling. The effects of IMC thickness ( $IMC_T$ ), solder joint width ( $SJ_W$ )  
111 and solder joint thickness ( $SJ_T$ ) on the thermo-mechanical reliability are also investigated for  
112 optimal parameter setting of the solder joints in crystalline silicon solar cell assembly. The  
113 solder joint formed using optimal parameter setting accumulates minimal creep strain energy  
114 density which leads to longer fatigue life.

## 115 116 **2. Solar cell assembly and reliability**

117 The structural design of solar cell assembly used in this study and a brief overview of solder  
118 joint reliability are presented in two parts: Structural design of solar cell assembly and solder  
119 joint reliability.

### 120 **2.1 Structural design of solar cell assembly**

121 The process of manufacturing conventional wafer-based crystalline silicon solar cell  
122 assembly begins with the use of silicon wafer as a base. Unto this base is deposited a layer of  
123 emitter material followed by the deposition of a layer of an anti-reflection coating (ARC).  
124 The function of the ARC layer is to ensure passage of all light to the silicon crystalline layers  
125 while minimizing reflection. Still, a transparent adhesive is deposited on the overlaid coating.  
126 Two layers of silver (Ag) in grid form are then printed on the cell's semiconductor material  
127 such that the metallization penetrates the ARC layer and makes contact with silicon wafer to  
128 form the front metal contact and to collect electric current generated. The printed Ag contacts  
129 are fired. Normally, aluminium contacts are also printed at the back surface of the cell  
130 material. Depicted in Fig. 1 is a typical schematic of cross-section of a laminated crystalline  
131 Si solar cell assembly. It consists basically of material layers including inter-metallic  
132 compounds. It can be observed from the figure that a rear contact material supports silicon  
133 wafer. The silicon wafer serves as a semiconductor consisting of a P-type layer at the rear and  
134 an N-type layer on the front. Crystalline silicon solar cells are interconnected with other cells  
135 in series and parallel to form a PV module of the required voltage and current. Figure 2  
136 shows a schematic of crystalline silicon solar cells interconnected in series with tabbing  
137 ribbon. The interconnection materials consist of copper ribbon, solder alloy and Ag busbar  
138 which have different coefficient of thermal expansion (CTE). The CTE mismatch induces  
139 thermo-mechanical stresses in the solder joint during soldering as well as during service  
140 operations resulting in fatigue and eventual failure. Therefore, robust packaging of the PV  
141 module is necessary to ensure the solder joint maintains integrity and reliability through  
142 subsequent manufacturing processes as well as during service conditions.

143

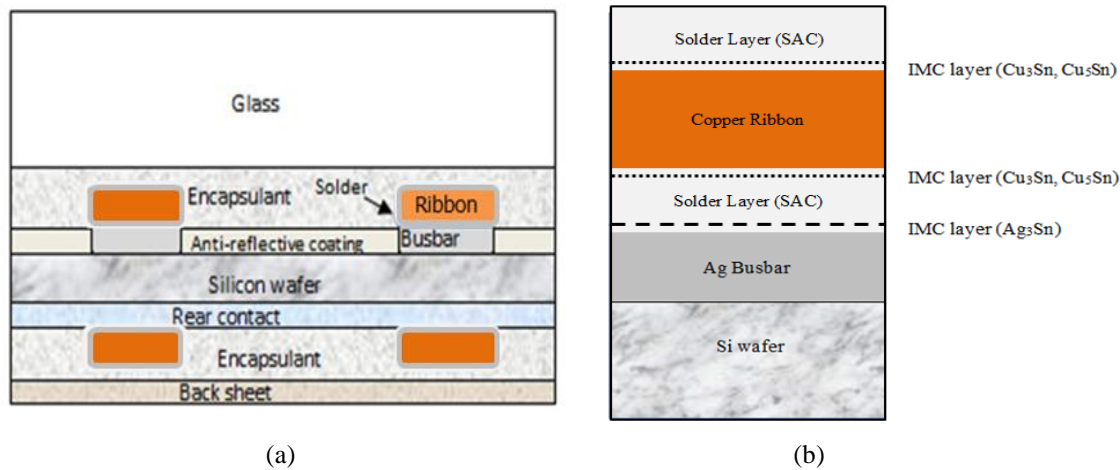


Fig. 1: Schematic of cross-section of typical crystalline Si solar cell assembly showing:  
 (a) encapsulated solar cell assembly (b) soldered interconnects including IMC layers

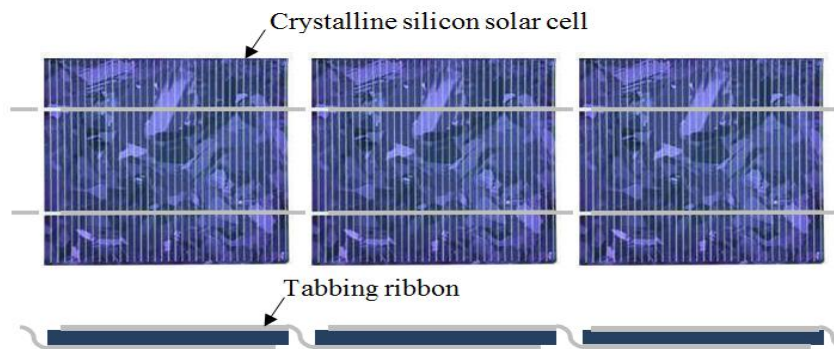


Fig. 2: Crystalline silicon solar cells interconnected in series with tabbing ribbon

## 2.2 Solder joint reliability

Crystalline silicon solar cells are interconnected to each other by soldering highly conductive copper ribbon strips to printed contacts at the front and back surfaces of the cells for current transfer from the front of one cell to the back of a neighbouring cell in a series connection [9] as shown in Fig. 2. As mentioned earlier, solder joints function as electrical connection, mechanical support and thermal conduit which implies that the reliability of solder joints can be affected by a variety of application conditions such as vibration, mechanical shock, thermo-mechanical fatigue, thermal aging and humidity [10]. In separate studies conducted, McCluskey [11] and Cuddalorepatta et al [12] reported that the soldered interconnect joint is the most susceptible part of the solar cell assembly. Besides, in a BP Solar study of PV module field failures, Wohlgemuth [13] reported that cell/interconnect break accounted for 40.7% of all types of field failures observed. The substantial field failures of interconnects demonstrate their criticality and the need to provide urgent solution to this challenge. This study is focussed on evaluating the critical design parameters of solder joints that impact thermo-mechanical reliability of the joints in crystalline silicon PV modules in order to optimize their designs.

## 3. Finite element modelling and simulation

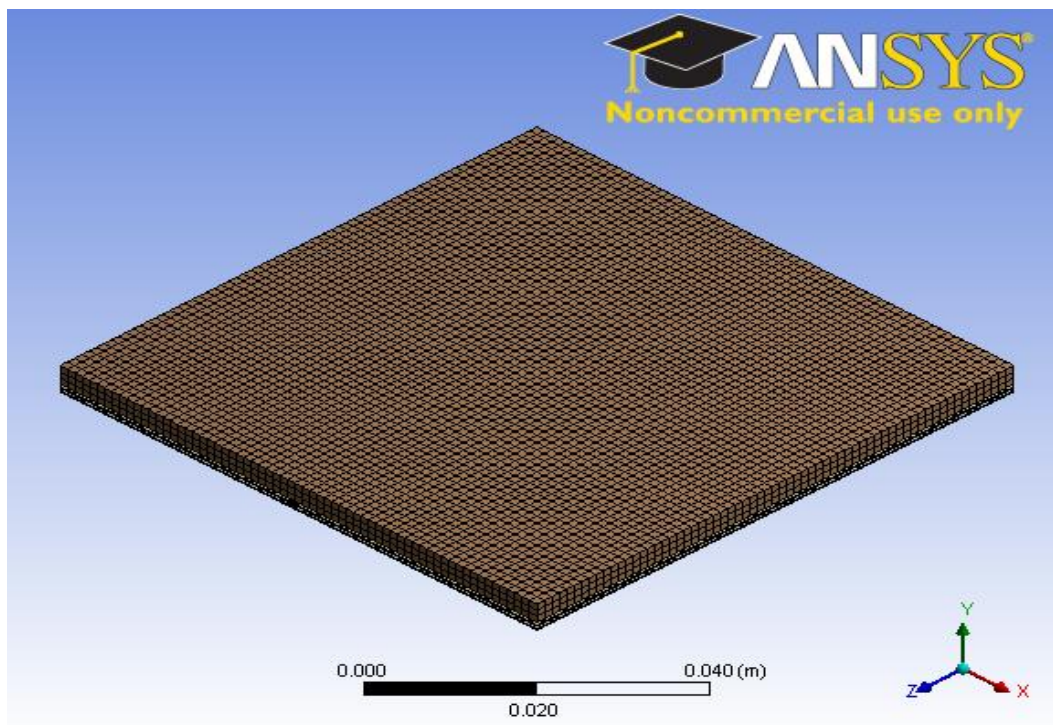
The study of thermo-mechanical reliability of solder joints in solar cell assembly subjected to thermal cycling using finite element modelling (FEM) is discussed in this section. The

172 section consists of three parts: Background and methodology; materials and their properties  
 173 and results of FEM.

### 174 3.1 Background and Methodology

175 This research utilized multi-crystalline silicon solar cell assembly with dimensions  $156 \times 156$   
 176  $\text{mm}^2$  to study induced stress, strain and strain energy in the assembly. The study was carried  
 177 out using commercial ANSYS academic research finite element package. A Bespoke Work  
 178 Station computer in the School of Engineering, University of Wolverhampton, UK was used  
 179 to execute the High Performance Computation (HPC) due to the magnitude of computations  
 180 involved. Also, in order to lessen modelling time and disc space, quarter symmetry of the  
 181 geometric models were simulated. Presented in Fig. 3 is a meshed geometric model of the  
 182 solar cell assembly with interconnected components. The model contains IMC layer at the  
 183 solder Cu ribbon interface and also at the solder Ag bus-bar interface. The IMC layer  
 184 thickness is assumed to be of the same thickness at each of the interfaces.

185  
 186



187  
 188  
 189  
 190  
 191

Fig. 3: Meshed crystalline Si solar cell assembly

192 It is worthy to note that in an experimental study, Schmitt et al [3] reported that the thickness  
 193 of IMC in a solar cell assembly can grow from about  $1\mu\text{m}$  to about  $12\mu\text{m}$  during thermal  
 194 cycling depending on the use of either leaded-solder or lead-free solder. Furthermore, in the  
 195 experimental investigation conducted by Schmitt et al [3] on lead-free SnAg3.5 solder, it was  
 196 found that IMC layer thickness grew up to  $4\mu\text{m}$ . Hence, in this study, IMC layer thickness of  
 197  $1\mu\text{m}$ ,  $2.5\mu\text{m}$  and  $4\mu\text{m}$  were used to build geometric models as these values are within the  
 198 experimental range. The solder joint formed during the interconnection of solar cells is of a  
 199 particular width and thickness depending on the manufacturer. The solder joint width used  
 200 ranges from  $1000\mu\text{m}$  to  $3000\mu\text{m}$  [12, 14, 15]. The solder joint width selected for the models  
 201 in this study are  $1000\mu\text{m}$ ,  $1200\mu\text{m}$  and  $1400\mu\text{m}$ . The smaller solder joints widths were  
 202 selected so as to minimize shadowing losses which will otherwise occur if wider ones are

203 selected. Likewise, various solder joint thickness are used by different manufacturers and are  
 204 usually between the range of 10 $\mu$ m and 40 $\mu$ m [16]. Based on this range of values, this study  
 205 used 20 $\mu$ m, 25 $\mu$ m and 30 $\mu$ m as solder joint thickness for the models.

206  
 207

### 208 3.2 Materials and their properties

209 The schematic cross-section of solar cell assembly presented in Fig. 1 shows that the solar  
 210 cell assembly consists of various materials with dissimilar properties. The main  
 211 interconnection materials are Sn3.8Ag0.7Cu solder, Cu ribbon, Ag bus-bar, IMCs and Si  
 212 wafer. These materials and their corresponding properties were assigned to the geometric  
 213 models built for this study. The mechanical properties of these materials such as Young's  
 214 modulus, CTE, Poisson ratio and shear modulus are presented in Table 1.

215

Table 1:  
 Mechanical properties of materials in solar cell assembly

Component	Young's modulus E (GPa)	CTE $\alpha$ ( $10^{-6}/^{\circ}\text{C}$ )	Poisson ratio $\nu$	Shear modulus G (GPa)
Glass [17]	73.3	8.5	0.21	30.289
Eva encapsulant [18]	0.011	270	0.4999	0.00367
Cu ribbon [19]	129	17	0.34	48.134
IMC [19]	110	23	0.3	42.308
Solder (Sn3.8Ag0.7Cu) [19]	43	23.2	0.3	16.538
Ag busbar [20]	72.4	10.4	0.37	26.423
Si wafer [21]	130	3.5	0.22	53.279
Al rear contact [20]	69	11.9	0.33	25.94
Tedlar backsheets [22]	1.4	30	0.4	0.5

216

#### 217 3.2.1 Constitutive solder model

218 Lead-free solder alloy has gained widespread application in electronics interconnection as a  
 219 response to the recommendation by the National Electronics Manufacturing Initiative  
 220 (NEMI) [23]. In this study the Sn3.8Ag0.7Cu Solder alloy is used and modelled as visco-  
 221 plastic material in solar cell assemblies experiencing both rate-dependent and rate-  
 222 independent inelastic deformation as it undergoes thermo-mechanical loading during  
 223 accelerated thermal cycling tests as well as in field service. The solder is assumed to exhibit  
 224 elastic, bilinear kinematic hardening after yield. The elastic and inelastic deformation  
 225 behaviour of the solder alloy is described by constitutive models. In this study, the Garofalo-  
 226 Arrhenius hyperbolic sine creep equation was employed in the finite element analysis (FEA)  
 227 to simulate the creep behaviour of the Sn3.8Ag0.7Cu solder joints. This equation in the  
 228 required format of input for implicit Garofalo-Arrhenius creep model is given by Syed [24]:

229

$$230 \quad \dot{\epsilon}_{cr} = C_1 [\sinh(C_2 \sigma)]^{C_3} \exp^{-C_4/T} \quad (1)$$

231 Where  $\dot{\epsilon}_{cr}$  is creep strain rate,  $C_1$ ,  $C_2$ ,  $C_3$  and  $C_4$  are constants for Sn3.8Ag0.7Cu solder and  
 232 T is the temperature in kelvins. The values of constants  $C_1$ ,  $C_2$ ,  $C_3$  and  $C_4$  for Sn3.8Ag0.7Cu  
 233 solder are given in the Table 2.

234

235

Table 2:  
Generalized Garofalo Creep Constants [24]

	Constant			
	C <sub>1</sub>	C <sub>2</sub>	C <sub>3</sub>	C <sub>4</sub>
Units	1/sec	1/Pa	-	K
Value	2.78E+05	2.45E-08	6.41	6500

236

237

### 238 3.2.2 Fatigue life prediction

239 The fatigue life of solder joints subjected to thermal cycling can be predicted using an energy  
240 density life prediction model. The model enables the calculation of number of repetitions or  
241 cycles to failure. The equation for calculating number of repetitions or cycles to failure using  
242 accumulated creep energy density per cycle is given by Syed [24]:

$$243 \quad N_f = (W' w_{acc})^{-1} \quad (2)$$

244 Where,  $N_f$  = Number of repetitions or cycles to failure

245  $W'$  = Creep energy density for failure and has a value of 0.0019

246  $w_{acc}$  = Accumulated creep energy density per cycle

247 In this study, the accumulated creep energy density per cycle is calculated using the volume-  
248 averaged method. The volume-averaged method has been widely used by researchers for the  
249 calculation of the accumulated creep energy density per cycle in solder joints [24-26]. The  
250 use of volume averaging technique minimizes the effect of mesh sensitivity as well as stress  
251 concentration on solder joint fatigue life prediction. The averaged strain energy density  
252 obtained through the volume-averaged method is given as [25, 26]:

253

$$254 \quad \Delta W_{ave} = \frac{\sum_i^n W_2^i \cdot V_2^i}{\sum_i^n V_2^i} - \frac{\sum_i^n W_1^i \cdot V_1^i}{\sum_i^n V_1^i} \quad (3)$$

255 Where  $W_2^i$ ,  $W_1^i$  is the total accumulated strain energy density in one element at the end point  
256 and the starting point of one thermal cycle respectively,  $V_2^i$ ,  $V_1^i$  is the volume of element at  
257 the end point and start point of one cycle respectively, and n is the number of selected  
258 elements to calculate averaged strain energy density.

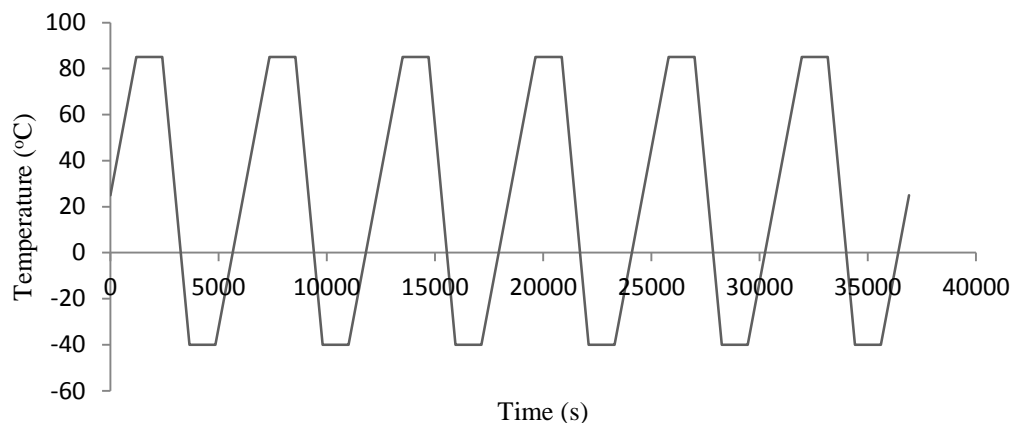
259

### 260 3.3 Loads and boundary conditions

261 Geometric models of crystalline silicon solar cell assembly were subjected to accelerated  
262 thermal cycling utilizing International Electro-technical Commission (IEC) 61215 standard

263 for photovoltaic panels to simulate thermal stresses on the materials of the models. The  
 264 models were subjected to six accelerated thermal cycling in 25 load steps between  $-40^{\circ}\text{C}$  to  
 265  $85^{\circ}\text{C}$ . The temperature loading started from  $25^{\circ}\text{C}$ , ramped up at a rate of  $3^{\circ}\text{C}/\text{min}$  to  $85^{\circ}\text{C}$ ,  
 266 where it had hot dwell for 20 min. It was then ramped down to  $-40^{\circ}\text{C}$  at a rate of  $6^{\circ}\text{C}/\text{min}$ ,  
 267 where it had cold dwell for 20 min. The thermal cycling profile is presented in Fig. 4 and it  
 268 was used to simulate actual cycling profile used during thermal load test. In the course of  
 269 such thermal load test, solder joints in crystalline solar cell assembly may crack as a result of  
 270 thermal fatigue [27].

271  
 272  
 273  
 274  
 275



276 Fig. 4: Plot of temperature profile of thermal load test condition used  
 277 in the solar cell assembly  
 278

279

## 280 4. Results and discussion

281 The optimization of solder joint parameter setting is discussed in this section. The section  
 282 consists of three parts: DOE using Taguchi method, main experiment as well as analysis and  
 283 discussion.

### 284 4.1 DOE using Taguchi method

285 Design of experiments (DOE) is a tool used by engineers and scientists to design and  
 286 develop products as well as to develop and improve processes [28]. Taguchi method for  
 287 DOE is based on quality philosophy aimed at the development of products and processes that  
 288 are robust to environmental factors and other sources of variability [28, 29]. Robustness in  
 289 this context is a measure of the ability of the product or process to perform consistently with  
 290 minimal effect from the uncontrollable noise factors due to operation or manufacturing. The  
 291 concept of signal-to-noise ratio is used to measure how the performance response varies  
 292 relative to the desired value under different noise conditions. Furthermore, the use of  
 293 Taguchi method for DOE substantially reduces product and process development lead time  
 294 and cost. The benefit of this method is that products and processes are developed which  
 295 perform better in the field and have higher reliability than those developed using other  
 296 methods.

297 This research utilized Taguchi method for DOE to study the thermo-mechanical reliability of  
 298 solder joints in solar cell assembly for optimal parameter design of the joints. The following  
 299 three control factors were chosen: IMC thickness ( $IMC_T$ ), solder joint width ( $SJ_W$ ) and solder  
 300 joint thickness ( $SJ_T$ ). Also, three DOE variables or levels designated as 1, 2 and 3 which  
 301 stand for low level, intermediate level and high level respectively are used in this study.  
 302 These control factors and levels are presented in Table 3.

303

Table 3:  
Control factors and levels

Control factor	Units	Level 1	Level 2	Level 3
A Intermetallic compound thickness ( $IMC_T$ )	$\mu\text{m}$	1	2.5	4
B Solder joint width ( $SJ_W$ )	$\mu\text{m}$	1000	1200	1400
C Solder joint thickness ( $SJ_T$ )	$\mu\text{m}$	20	25	30

304

305 Creep strain energy density is a robust damage indicator of solder joint as it is based on the  
 306 deformation internally stored throughout the volume of the joint during thermal loading. As a  
 307 result, accumulated creep strain energy density is used in solder joint life prediction models  
 308 [24]. In this study, the change in accumulated creep strain energy density  $\Delta\omega_{acc}$ , of the solder  
 309 joint is chosen as the quality or response factor and used in the Taguchi DOE for  
 310 optimization. The objective of this optimization is to minimize the accumulated creep strain  
 311 energy density  $\Delta\omega_{acc}$ , in the solder joint as the decrease in  $\Delta\omega_{acc}$  means the enhancement of  
 312 thermo-mechanical reliability. Minimization of  $\Delta\omega_{acc}$  aims at making the system response as  
 313 small as possible by obtaining the smaller-the-better signal-to-noise ratio. To achieve this  
 314 aim, the absolute magnitude of the smaller-the-better signal-to-noise (S/N) ratio is chosen and  
 315 is mathematically defined as [5, 29]:

316

$$317 \quad S/N = -10 \log \left( \frac{\sum_{i=1}^n y_i^2}{n} \right) \quad (4)$$

318

319 where  $y_i$  is the  $i^{\text{th}}$  value of the quality characteristic and  $n$  is the number of values. In this  
 320 case, the value of the quality characteristic is taken to be  $y \equiv \Delta\omega_{acc}$ . Besides, since a  
 321 numerical analysis does not create data variations, then  $n = 1$ . Hence, the equation of the  
 322 signal-to-noise ratio transforms to:

323

$$324 \quad S/N = -10 \log (\Delta\omega_{acc})^2 \quad (5)$$

325

326 The calculation of the chosen S/N ratio is through the Taguchi DOE method based on  
 327 orthogonal arrays. Orthogonal array is an arrangement of numbers in columns and rows in  
 328 such a way that each column represents a factor while the rows represent levels of the factors  
 329 [29]. The factors affect the outcome of the process under study. In this study, the  $L_9$  ( $3^3$ )  
 330 orthogonal array is applied to Taguchi DOE to investigate the effects of IMC thickness  
 331 ( $IMC_T$ ), solder joint width ( $SJ_W$ ) and solder joint thickness ( $SJ_T$ ) on the thermo-mechanical  
 332 reliability of solder joints. Presented in Table 4 is a table of Taguchi DOE (Orthogonal array  
 333  $L_9$ ) showing nine models and their respective solder joint parameter level. ANSYS  
 334 DesignModeller was used to build the geometric model of each designed model using their  
 335 respective parameter setting.

336

337 To obtain the optimal parameter setting of solder joint in solar cell assembly, a main  
 338 experiment must be implemented. The implementation of the main experiment commences  
 339 with setting the parameter for each experimental run. Thus, each design of the solder joint is  
 340 assigned its respective parameter setting as shown in Table 4. The geometric models of the  
 341 solar cell assembly containing the solder joint are subsequently built with the appropriate  
 342 parameter setting.

343

Table 4:  
 Table of Taguchi DOE (Orthogonal array L<sub>9</sub>)

Model number	Factor and level			Parameter setting
	A	B	C	
1	1 <sub>(1)</sub>	1 <sub>(1000)</sub>	1 <sub>(20)</sub>	A1B1C1
2	1 <sub>(1)</sub>	2 <sub>(1200)</sub>	2 <sub>(25)</sub>	A1B2C2
3	1 <sub>(1)</sub>	3 <sub>(1400)</sub>	3 <sub>(30)</sub>	A1B3C3
4	2 <sub>(2.5)</sub>	1 <sub>(1000)</sub>	2 <sub>(25)</sub>	A2B1C2
5	2 <sub>(2.5)</sub>	2 <sub>(1200)</sub>	3 <sub>(30)</sub>	A2B2C3
6	2 <sub>(2.5)</sub>	3 <sub>(1400)</sub>	1 <sub>(20)</sub>	A2B3C1
7	3 <sub>(4)</sub>	1 <sub>(1000)</sub>	3 <sub>(30)</sub>	A3B1C3
8	3 <sub>(4)</sub>	2 <sub>(1200)</sub>	1 <sub>(20)</sub>	A3B2C1
9	3 <sub>(4)</sub>	3 <sub>(1400)</sub>	2 <sub>(25)</sub>	A3B3C2

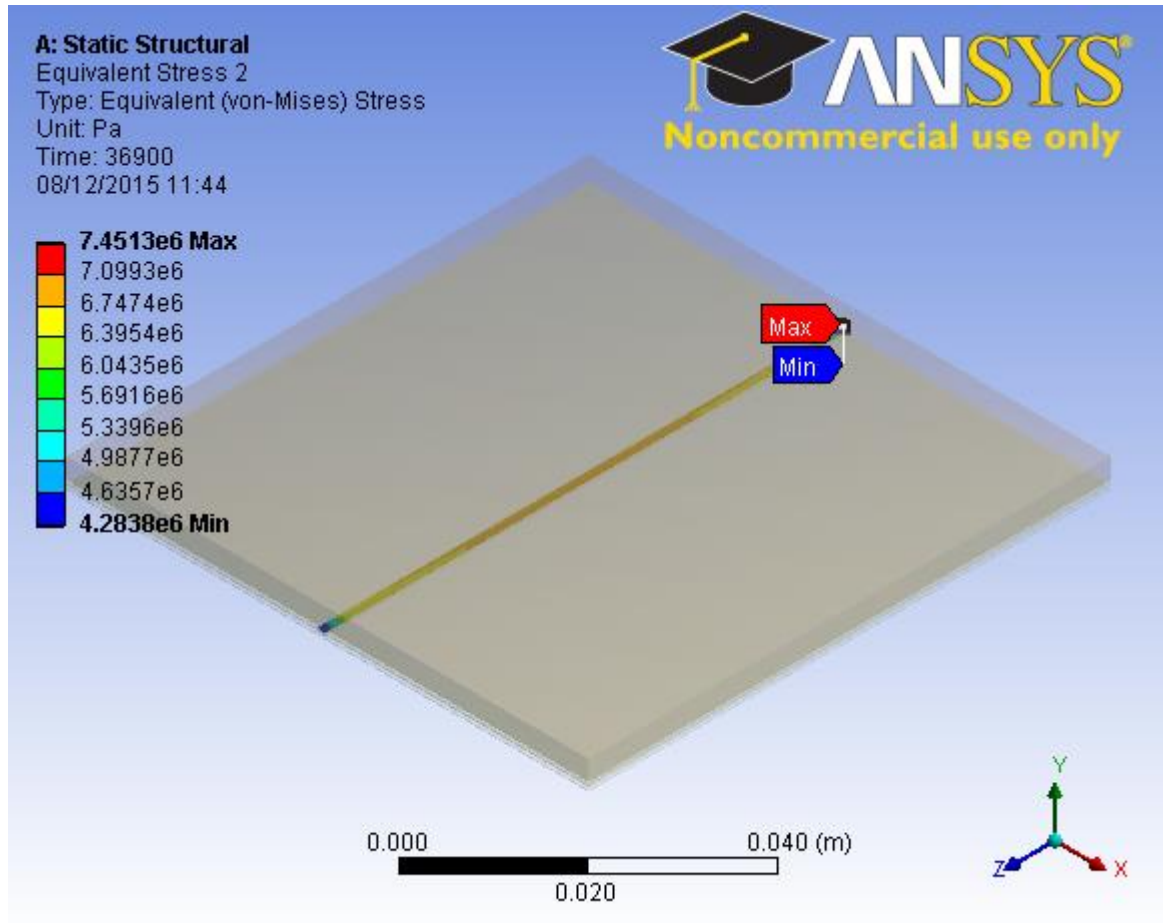
344

#### 345 4.2 Results of FEM

346 Solder interconnect in the solar cell assembly is the critical constituent for consideration of  
 347 thermo-mechanical reliability of the assembly. Therefore, optimizing the geometry  
 348 parameters of solder joint is key to enhancing the thermo-mechanical reliability of the solder  
 349 interconnects. Accordingly, the response of solder joint to thermal cycling is required to  
 350 provide an insight to solder behaviour. Thus simulation results showing stress, creep strain  
 351 and strain energy provide useful information on the behaviour of solder joints. In this study,  
 352 nine original geometric models were built and simulated using ANSYS academic research  
 353 finite element package. Presented in Fig. 5 are simulation results of damage distribution of  
 354 solder joint in solar cell assembly for one of the models. The figure shows equivalent stress,  
 355 equivalent creep strain and strain energy in the solder joint. The maximum damage  
 356 distribution is at the right side edge, towards the right side edge and at the mid-section of the  
 357 solder joint for stress, creep strain and strain energy respectively. This indicates that crack  
 358 initiation and propagation is most likely to occur at the mid-section of the solder joint and  
 359 will eventually lead to fatigue failure at that preferential failure site. A close observation of  
 360 Fig. 5(b) reveals that the maximum creep strain damage is located at the lower side of the  
 361 solder joint adjacent to silver (Ag) bus-bar which is at a similar location to a cracked solder  
 362 joint in crystalline solar cell assembly shown in Fig. 6.

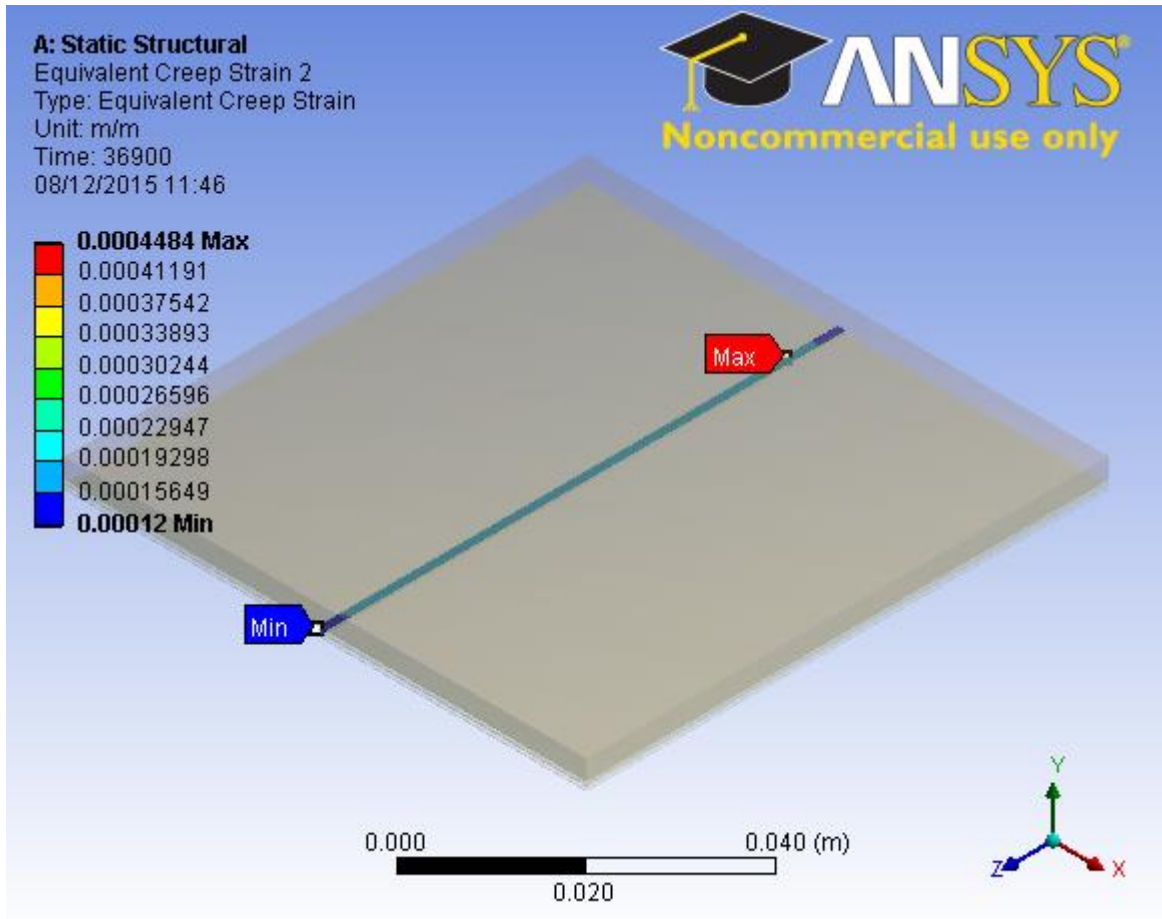
363

364

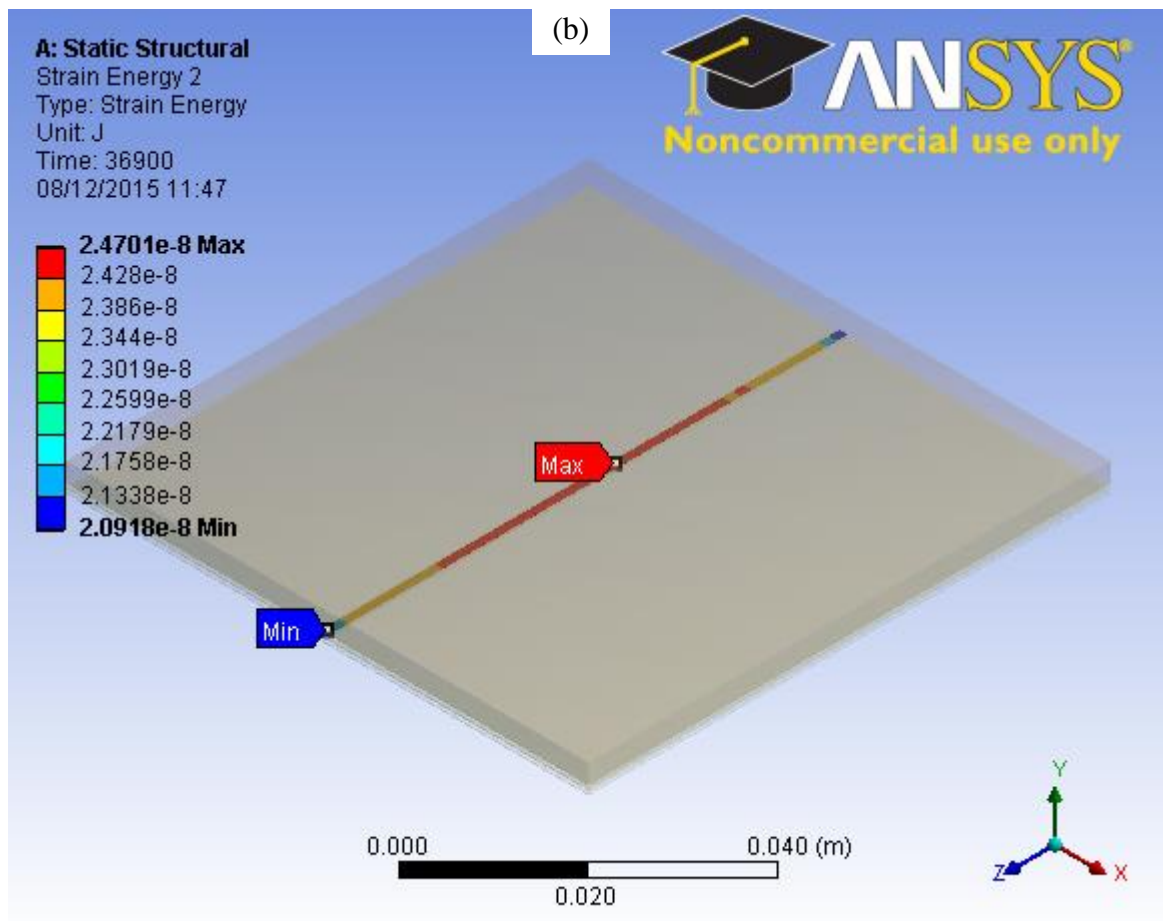


365  
366  
367  
368  
369

(a)



370  
371

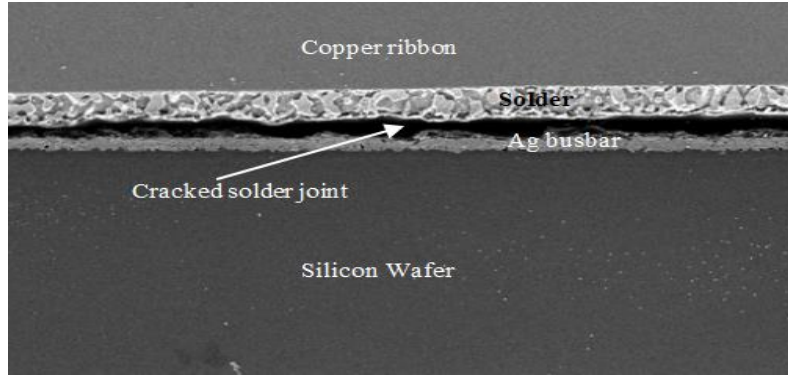


372

373  
374  
375  
376  
377

(c)

Fig. 5: Damage distribution in solder joint of the solar cell assembly showing:  
(a) Equivalent stress (b) Equivalent creep strain (c) Strain energy

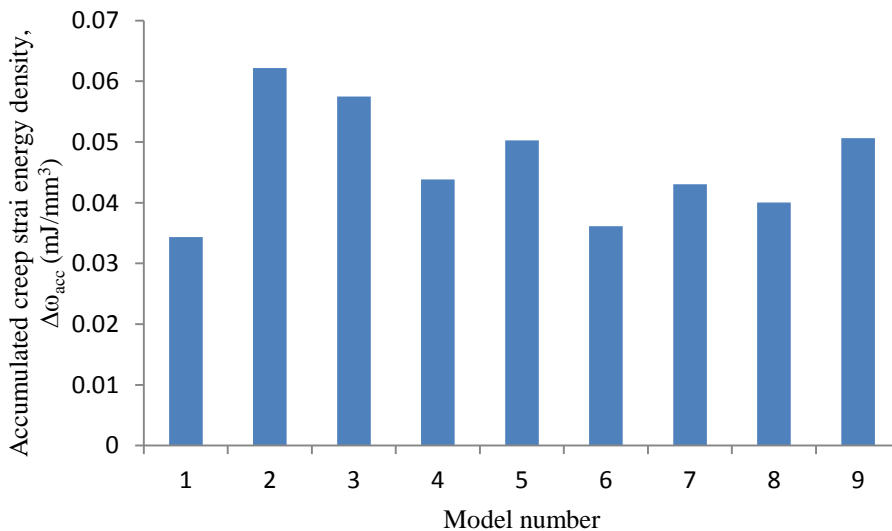


378  
379  
380

Fig. 6: Cracked solder joint in crystalline solar cell assembly [27]

381 The plot of accumulated change in creep strain energy density against model number is  
382 presented in Fig. 7. It can be observed from Fig. 7 that model number 2 has the largest  
383 accumulated change in creep strain energy density ( $\Delta\omega_{acc}$ ) compared to all the other models.  
384 This implies that the solder joint in model number 2 is the most susceptible to failure  
385 compared to the others. Therefore, model number 2 has the most critical solder joint and  
386 hence, is the worst original design compared to the other models.

387



388  
389  
390

Fig. 7: Plot of accumulated creep strain energy density against model number

391 The geometric models were simulated and accumulated creep strain energy density  
 392 determined from simulation results for each design. The predicted results as well as the  
 393 computed S/N ratio for each design are presented in Table 5.

394

Table 5:  
 Experimental results and S/N ratio

Model number	Factor and level			Quality/Response	S/N ratio
	A	B	C	$\Delta\omega_{acc}$ (mJ/mm <sup>3</sup> )	
1	1	1	1	0.03436	29.28
2	1	2	2	0.06218	24.13
3	1	3	3	0.05750	24.81
4	2	1	2	0.04384	27.16
5	2	2	3	0.05028	25.97
6	2	3	1	0.03613	28.84
7	3	1	3	0.04303	27.32
8	3	2	1	0.04002	27.95
9	3	3	2	0.05061	25.92
<b>Average</b>					<b>26.82</b>

395

396

#### 397 4.3 Analysis and discussion

398 In this analysis, minimization of the response is desired for accumulated creep strain energy  
 399 density,  $\Delta\omega_{acc}$  in the solder joint. The averaged effect response for S/N ratio of each factor  
 400 was investigated to determine the contributions of IMC thickness, solder joint width and  
 401 solder joint thickness on the solder joint thermo-mechanical reliability. Minitab 17 statistical  
 402 software was used to carry out analysis of variance (ANOVA) on the data presented in Table  
 403 5. The main effect plots from ANOVA are shown in Fig. 8 and consist of the plot for IMC  
 404 thickness, solder joint width and solder joint thickness. Also, presented in Table 6 is the S/N  
 405 response and rank for the three factors.

406 The means of S/N ratio presented in Table 6 and plotted in Fig. 8 are obtained using the data  
 407 in Table 5 and applying Eq. 6 for each factor.

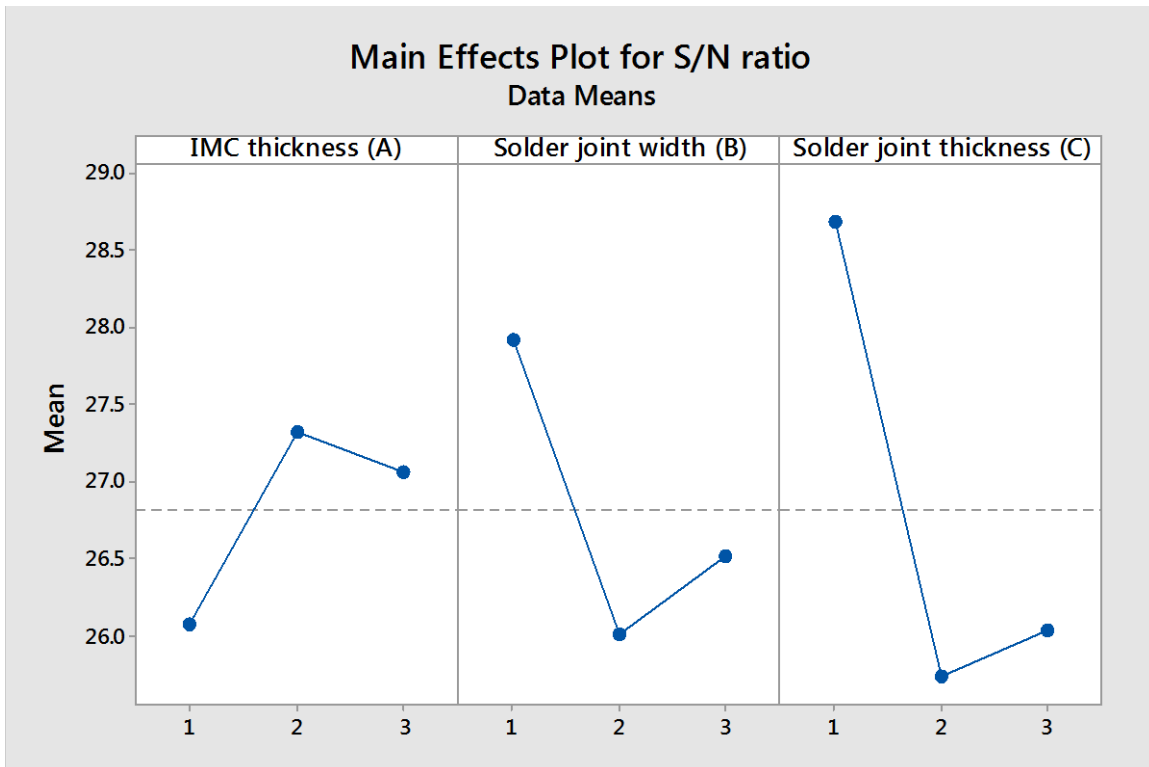
$$408 \quad \bar{j}_i = \frac{1}{n} \sum_{j=1}^n j_i \Big|_{\forall j,i} \quad (6)$$

409 Where  $j$  may be designated as A, B or C represent factor and  $i$  stand for values 1, 2 or 3  
 410 represent the level. The symbols  $\bar{j}_i$  and  $n$  are the mean of S/N ratio and the number of level in  
 411 the experiment respectively. The sign  $\Big|_{\forall j,i}$  denotes that Eq. 6 is evaluated at  $j$  and  $i$  values.  
 412 These means represent the factor average effects at each level. Furthermore, with reference to  
 413 Table 6, the effect of a factor ( $E_j$ ) is the observed range in its level. It can be represented as:

414  $E_j = F_{jmax} - F_{jmin} \Big|_{v_i}$  (7)

415 Where  $E_j$ , is effect of factor  $j$  and  $F_{jmax}$  and  $F_{jmin}$ , are maximum and minimum value of factor  
 416  $j$ , respectively. The sign  $\Big|_{v_i}$  designates that Eq. 7 is evaluated across the level.

417  
 418  
 419  
 420  
 421  
 422  
 423  
 424  
 425  
 426



427  
 428 Fig. 8: Main effect plot of IMC thickness, solder joint width and solder joint thickness

429  
 430

Table 6:  
S/N response and rank

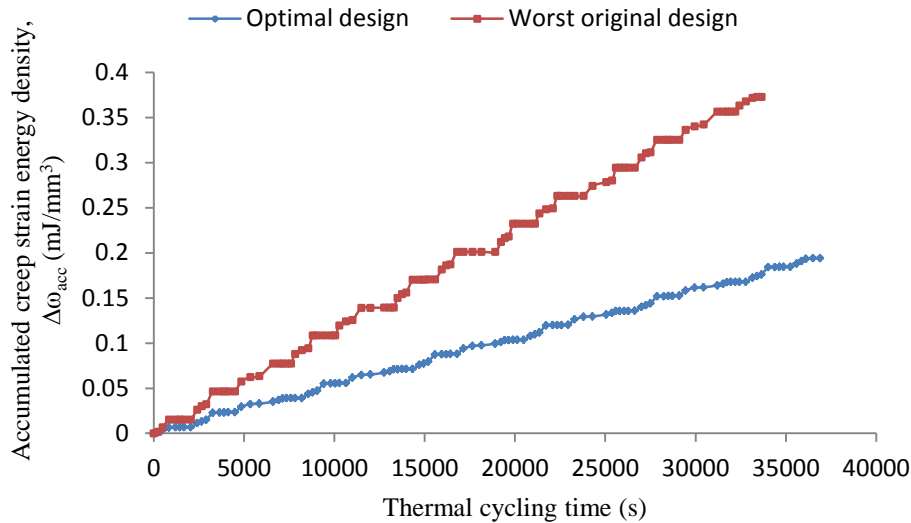
	Factor and level		
	A	B	C
Level 1	26.07	27.92	28.69
Level 2	27.32	26.02	25.74
Level 3	27.06	26.52	26.03
Effect	1.25	1.90	2.95
Rank	3	2	1

431

432 Results from Fig. 8 and Table 6 indicate that the most significant parameter for the thermo-  
 433 mechanical reliability of solder joint is Factor C (solder joint thickness) as it has the largest  
 434 effect, hence is ranked 1<sup>st</sup>. Factor A (IMC thickness) is the least significant as it has the least  
 435 effect, hence ranked 3<sup>rd</sup>. Factor B (solder joint width) has the second largest effect as it is  
 436 ranked 2<sup>nd</sup>. Furthermore, from Table 6, the optimal parameter setting based on maximum  
 437 values is deduced to be A2B1C1 which reveal that the solder joint should have an IMC  
 438 thickness of 2.5 $\mu$ m, width of 1000 $\mu$ m and thickness of 20 $\mu$ m.

439 A geometric model of solar cell assembly containing solder joint with the optimal parameters  
 440 was built and simulated in order to provide results for confirmation and comparison with  
 441 worst original design (Model 2). Accumulated creep strain energy density was computed  
 442 from the simulation results of the optimal design and S/N ratio was computed as well.  
 443 Presented in Fig. 9 is comparison of accumulated creep strain energy density of worst  
 444 original design and optimal design. It can be observed from Fig. 9 that accumulated creep  
 445 strain energy density in solder joint of worst original design is higher than that of optimal  
 446 design. This implies that the optimal design makes the solder joint more robust than the worst  
 447 original design. Comparison of the accumulated creep strain energy density,  $\Delta\omega_{acc}$  and the  
 448 S/N ratio of the worst original design and the optimal design are presented in Table 7. It can  
 449 be observed from Table 7 that the optimal design has the smallest accumulated creep strain  
 450 energy density,  $\Delta\omega_{acc}$  compared to all the other original designs. Furthermore, the optimal  
 451 design reduces the  $\Delta\omega_{acc}$  by 47.96% compared to that of the worst original design thereby  
 452 improving the thermo-mechanical reliability of the solder joints in crystalline silicon solar  
 453 cell assembly.

454



455

456

Fig. 9: Comparison between accumulated creep strain energy density of original design and optimal design

457

458

Table 7:  
Comparison of  $\Delta\omega_{acc}$  in worst original and optimal designs

	Factors and level			$\Delta\omega_{acc}$ (mJ/mm <sup>3</sup> )	S/N ratio
	A	B	C		
Worst original design	1	2	2	0.06218	24.13
Optimal design	2	1	1	0.03236	29.80
Reduction				47.96%	

459

460

461

462

463 Furthermore, Eq. 2 was used to compute fatigue life of the solder joints in worst original  
 464 design as well as in optimal design and the results are shown in Fig. 10. In addition, the  
 465 expected life of PV modules which is 13688 cycles to failure (25 years) as discussed in  
 466 section 1 is included in Fig. 10. Besides, in an experimental study, Kumar and Sarkar [30]  
 467 tested 20 PV modules for stress failure and obtained the least survival life to be 21 years  
 468 (11497 cycles to failure). This experimental test life is also presented in Fig. 10.

469

470

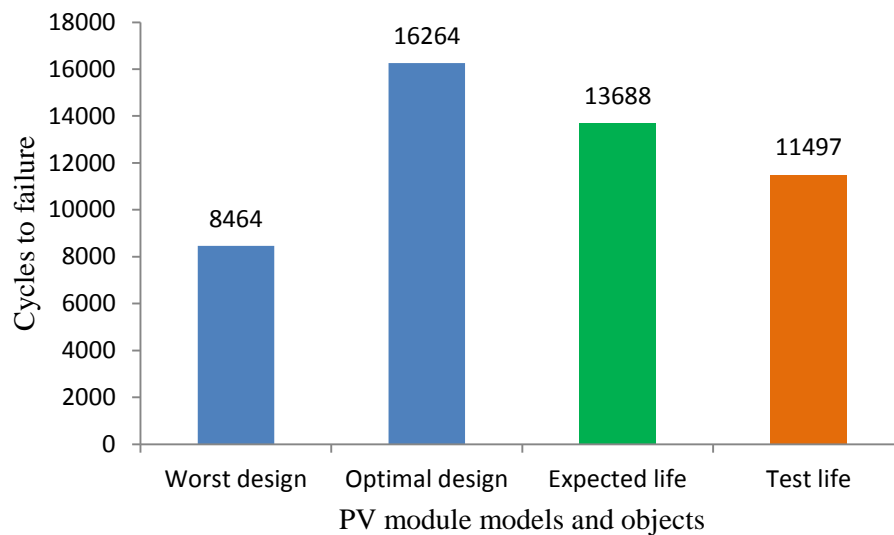


Fig. 10: Predicted cycles to failure of solder joint models compared with expected and test values

It can be observed from Fig. 10 that the predicted solder joint fatigue life of the optimal design is almost double that of the worst original design and higher than the expected life of PV modules. This implies that the solder joint of the optimal design has topmost thermo-mechanical reliability which is very desirable for the PV modules.

## 5. Conclusions

An investigation of the thermo-mechanical reliability of solder joints in crystalline silicon solar cell assembly using finite element modelling (FEM) and Taguchi method for DOE is reported in this paper. The investigation aims to study the effect of intermetallic compound (IMC) thickness, solder joint width and solder joint thickness on the thermo-mechanical reliability of Sn<sub>3.8</sub>Ag<sub>0.7</sub>Cu solder joint with various sets of parameters and subjected to thermal cycling. The focus of this investigation is to minimize accumulated change in creep strain energy density and optimize the parameter setting of solder joint towards the enhancement of thermo-mechanical reliability of the joint.

The results of simulation carried out reveal that the maximum damage distribution is at the mid-section of the solder joint for stress, creep strain and strain energy. The maximum creep strain damage is located at the lower side of the solder joint adjacent to silver (Ag) busbar. This indicates that crack initiation and propagation is most likely to occur at the mid-section of the solder joint and will eventually lead to fatigue failure at that preferential failure site.

Furthermore, the outcomes of this investigation show that the magnitude of accumulated change in creep strain energy density depends on the parameter setting of solder joint. Comparison of the main effects of IMC thickness, solder joint width and solder joint thickness on the thermo-mechanical reliability of the solder joint indicates that solder joint thickness has the most significant effect.

The analysis of parameters selected towards thermo-mechanical reliability improvement of solder joint produced an optimal parameter setting which will make the joint robust. The

505 optimal parameter setting for the solder joint is that the solder joint thickness is 20 $\mu$ m, solder  
506 joint width is 1000 $\mu$ m and IMC thickness is 2.5 $\mu$ m. Also, the optimal parameter setting  
507 improves the performance of the solder joint by 47.96% compared to the worst case original  
508 parameter setting. Interestingly, the optimized model is predicted to have 16264 cycles to  
509 failure which is higher than the expected 13688 cycles to failure of a PV module designed to  
510 last for 25 years.

511 Based on these findings, the authors recommend that manufacturers of wafer-based  
512 crystalline silicon photovoltaic modules use this study to analyse and optimize their designs  
513 in order to enhance the thermo-mechanical reliability of solder joints.  
514

## 515 **Acknowledgements**

516 The authors acknowledge funding provided by the Petroleum Technology Development Fund  
517 (PTDF), Nigeria used in carrying out this study.  
518

## 519 **References**

- 520 [1] Burger B, Kiefer K, Kost C, Nold S, Phillips S, Preu R, et al. Photovoltaic Report,  
521 Fraunhofer Institute for Solar Energy Systems ISE, Freiburg, Germany, 2014; 1-42.
- 522 [2] Guyenot M, Peter E, Zerrer P, Kraemer F, Wiese S. Enhancing the lifetime prediction  
523 methodology for photovoltaic modules, Proceedings of 12<sup>th</sup> Int. Conf. on Thermal,  
524 Mechanical and Multiphysics Simulation and Experiments in Microelectronics and  
525 Microsystems, Linz, Austria, 2011; 1-4.
- 526 [3] Schmitt P, Kaiser P, Savio C, Tranitz M, Eitner U. Intermetallic Phase Growth and  
527 Reliability of Sn-Ag-Soldered Solar Cells, Energy Procedia, 2012; 27:664-669.
- 528 [4] Che FX, Pang JHL. Characterization of IMC layer and its effect on thermomechanical  
529 fatigue life of Sn-3.8Ag-0.7Cu solder joints, Journal of Alloys and Compounds, 2012;  
530 541:6-13.
- 531 [5] Huan Y, Xue S, Zhang L, Ji F, Dei W. Reliability evaluation of CSP soldered joints  
532 based on FEM and Taguchi method, Computational Materials Science, 2010; 48:509-  
533 512.
- 534 [6] Ladani LJ. Numerical analysis of thermo-mechanical reliability of through silicon vias  
535 (TSVs) and solder interconnects in 3-dimensional integrated circuits, Microelectronics  
536 Engineering, 2010; 87:208-215.
- 537 [7] Yang P, Tan G. Taguchi-numerical approach on thermo-mechanical reliability for  
538 PBGA, International Journal of Numerical Modelling: Electronic Networks, Devices and  
539 Fields, 2010; 24:437-447.
- 540 [8] Taguchi G. Quality Engineering (Taguchi Methods) For The Development of Electronic  
541 Circuit Technology, IEEE Transactions on Reliability, 1995; 44:225-229.
- 542 [9] Jeong J, Nochang P, Wonsik H, Changwoon H. Analysis for the Degradation Mechanism  
543 of Photovoltaic Ribbon Wire under Thermal Cycling, Proceedings of 37<sup>th</sup> Photovoltaic  
544 Specialists Conference, Seattle, WA. USA, 2011; 003159-003161.
- 545 [10] Lechovič E, Erika H, Beáta S, Ingrid K, Koloman U. Solder Joint Reliability,  
546 <[https://www.mtf.stuba.sk/docs/internetovy\\_casopis/2009/1/hodulova.pdf](https://www.mtf.stuba.sk/docs/internetovy_casopis/2009/1/hodulova.pdf)> (accessed  
547 March 12, 2013).
- 548 [11] McCluskey FP. Reliability Modeling for Photovoltaic Modules, Proceedings of  
549 Photovoltaic Module Reliability Workshop, Denver, Colorado, 2010.

- 550 [12] Cuddalorepatta G, Abhijit D, Scott S, Jerome M, Todd T, James L. Durability of Pb- free  
551 solder between copper interconnect and silicon in photovoltaic cells, Progress in  
552 Photovoltaics: Research and Applications, 2010; 18(3):168-182.
- 553 [13] Wohlgenuth JH. Reliability of Photovoltaic Cells, Modules, Components, and Systems,  
554 Proceedings of SPIE conference, 7048, 2008.
- 555 [14] Klengel R, Härtel R, Schindler S, Schade D, Sykes B. Evaluation of the Mechanical  
556 Strength of Solar Cell Solder Joint Interconnects and Their Microstructural Properties by  
557 Developing a New Test and Inspection Equipment, 26th European Photovoltaic Solar  
558 Energy Conference and Exhibition, Hamburg, Germany, 2011; 1507-1511.
- 559 [15] Gierrth P, Rebenklau L, Michaelis A. Evaluation of Soldering Processes for High  
560 Efficiency Solar Cells, 35th International Spring Seminar on Electronics Technology,  
561 Vienna, Austria, 2012; 133-137.
- 562 [16] Rogelj I, Ziger P, Eiselt P. PV Ribbon: Overview of Product Specifications and  
563 Comparison of Production Processes, SOLARCON, Shanghai, China, 2012.
- 564 [17] Webb JE, Hamilton JP. Physical Properties of Glass and the Requirements for  
565 Photovoltaic Modules, Proceedings of Photovoltaic Module Reliability Workshop,  
566 Golden, Colorado, USA, 2011; 1-18.
- 567 [18] Eitner U, Pander M, Kajari-Schröder S, Köntges M, Altenbach H. Thermomechanics of  
568 PV Modules Including the Viscoelasticity of Eva, Proceedings of 26th European  
569 Photovoltaic Solar Energy Conference and Exhibition, Hamburg, Germany, 2011; 3267-  
570 3269.
- 571 [19] Amalu EH, Ekere NN. High temperature reliability of lead-free solder joints in a flip  
572 chip assembly, Journal of Materials Processing Technology, 2012; 212:471-483.
- 573 [20] The Engineering Toolbox, <[http://www.engineeringtoolbox.com/young-modulus-  
574 d\\_417.html](http://www.engineeringtoolbox.com/young-modulus-d_417.html)> (accessed November 6<sup>th</sup>, 2015).
- 575 [21] Hopcroft MA, Nix WD, Kenny TW. What is the Young's Modulus of Silicon?, Journal  
576 of Microelectromechanical Systems, 2010; 19( 2):229-238.
- 577 [22] Wiese S, Kraemer F, Peter E, Seib J. Mechanical Problems of novel Back Contact Solar  
578 Modules, Proceedings of 13th International Conference on Thermal, Mechanical and  
579 Multi-Physics Simulation and Experiments in Microelectronics and Microsystems,  
580 EuroSimE, Cascais, near Lisbon, Portugal, 2012.
- 581 [23] Che FX, Pang JHL, Xiong BS, Xu L, Low TH. Lead Free Solder Joint Reliability  
582 Characterization for PBGA, PQFP AND TSSOP Assemblies, Proceedings of 55<sup>th</sup> ECTC,  
583 Florida, USA, 2005; 916-921.
- 584 [24] Syed A. Accumulated Creep Strain and Energy Density Based Fatigue Life Prediction  
585 Models for SnAgCu Solder Joints, Proceedings of 54<sup>th</sup> ECTC, Las Vegas, USA, 2004;  
586 737-746.
- 587 [25] Pang JHL, Che FX. Isothermal Cyclic Bend Fatigue Test Method for Lead Free Solder  
588 Joints, Proceedings of 10<sup>th</sup> Intersociety Conference on Thermal and Thermomechanical  
589 Phenomena in Electronics Systems, San Diego, California, USA, 2006; 1011-1017.
- 590 [26] Che FX, Pang JHL. Fatigue Reliability Analysis of Sn-Ag-Cu Solder Joints Subject to  
591 Thermal Cycling, IEEE Transaction on Device and Materials Reliability, 2012; 13(1):36-  
592 49.
- 593 [27] Jeong JS, Park N, Han C. Field Failure Mechanism Study of Solder Interconnection for  
594 Crystalline Silicon Photovoltaic Module, Microelectronics Reliability, 2012; 52:2326-  
595 2330.
- 596 [28] Montgomery DC. Design and Analysis of Experiments, John Wiley & Sons, Inc.; 2013.
- 597 [29] Davies R, Coole T, Osypiw D. A Review of Traditional and Taguchi Design of  
598 Experiments: Devising a Method Selection Criteria, Proceedings of 25<sup>th</sup> Flexible  
599 Automation and Intelligent Manufacturing, Wolverhampton, UK, 2015; 308-315.

- 600 [30] Kumar S, Sarkar B. Design for Reliability with Weibull Analysis for Photovoltaic  
601 Modules, International Journal of Current Engineering and Technology, 2013; 3(1):129-  
602 134.